



Published in final edited form as:

Biomaterials. 2009 November ; 30(33): 6530–6540. doi:10.1016/j.biomaterials.2009.08.019.

In vitro Model of Mesenchymal Condensation During Chondrogenic Development

Sourabh Ghosh^{a,b}, Michael Laha^a, Sourav Mandal^b, Sejuti Sengupta^a, and David L Kaplan^{a,*}

^a Department of Biomedical Engineering, Tufts University, Boston, USA

^b Department of Textile Technology, Indian Institute of Technology, Delhi, India

Abstract

Mesenchymal condensation is a pre-requisite of chondrogenesis during embryonic development. The current understanding of chondrogenesis is limited in terms of chondrogenic condensation mechanisms. In particular, the role of matrix stiffness on homotypic cell-cell interactions leading to the establishment of distinct aggregated chondrogenic morphology from mesenchymal cells is unclear. An in vitro biomaterials-based model to assess the interactions of matrix stiffness on chondrogenesis is described herein, where by sensing subtle variation in morphology and stiffness of nanofibrous silk protein matrixes human mesenchymal stem cells migrated and assumed aggregated morphologies, mimicking early stage chondrogenesis. This simple in vitro model system has potential to play a significant role to gain insight into underlying mechanisms of mesenchymal condensation steps during chondrogenesis, integrating concepts of developmental biology, biomaterials and tissue engineering.

Keywords

Electrospinning; chondrogenesis; in vitro model system; condensation

1. Introduction

During the past decade tissue engineering research has progressed towards regenerating functional tissues using cells with designer scaffolds to restore or replace lost morphology and functions of diseased or damaged organs. Despite this progress, thus far only a few products have reached human clinical trials [1]. As a paradigm shift, related emerging trends in the field include establishing in vitro human disease model systems in order to gain fundamental insight into pathological conditions [2,3], and simulating complex biological processes during tissue development in vitro for future regeneration or repair strategies [4-6]. Cartilage tissue engineering in vitro has generated insight about involvement of several factors in inducing chondrogenic differentiation, such as hypoxia [7], high cell densities [8], changes in cytoskeleton and cell shape [9-11], presence of specific soluble factors [12,13], and modulation in expression patterns of selected transcription factors, e.g., N-cadherin, neural cell adhesion molecule (N-CAM, CD56), SRY (sex determining region Y)-box 9 (Sox-9), Bone

Corresponding Author: david.kaplan@tufts.edu; 617-627-3251.

Publisher's Disclaimer: This is a PDF file of an unedited manuscript that has been accepted for publication. As a service to our customers we are providing this early version of the manuscript. The manuscript will undergo copyediting, typesetting, and review of the resulting proof before it is published in its final citable form. Please note that during the production process errors may be discovered which could affect the content, and all legal disclaimers that apply to the journal pertain.

morphogenic proteins, among others. Further, understanding is improving how underlying matrix stiffness [14,15] can guide stem cells towards a specific developmental lineage, but matrix stiffness alone is likely to be insufficient to achieve complete terminal differentiation [14].

The extracellular matrix (ECM) secreted by cells are macromolecules with nanofibrillar features. The ECM plays a crucial role in tissue development, by providing a natural 'scaffold' to guide cell responses, in terms of regulation of cell anchorage, migration, organization and triggering signals that govern cell survival, cell cycle progression and expression of differentiated phenotypes during development. Basement membranes (BM) are 50-100 nm thick nano-fibrous sheet-like ECM architectures that underpin epithelial and endothelial cells. BM is also found supporting several mesenchymal cell types, such as smooth muscle cells, adipocytes- the cells which are derived from the same progenitor cells as chondrocytes. A new generation of nanofibrillar biomaterials are being pursued which simulate typical morphologies of ECMs or BMs [16]. These elegantly designed synthetic systems also offer microenvironments suitable for cell and tissue function by providing spatial and temporal signals, and affecting mechanotaxis, chemotaxis, haptotaxis, durotaxis processes influencing tissue regeneration [17,18]. However, despite this progress, the quantitative relationships between matrix morphology, integrin expression patterns, focal adhesion-actin coupling dynamics, cellular motility and targeted differentiation capacity are still not well understood. Thus, understanding how artificial ECM nanofibrous architectures, in terms of mechanical flexibility, dictate cell fate and stem cell differentiation will facilitate progress in exploiting these systems toward specific tissue goals in vitro and in vivo.

Chondrocytes are terminally differentiated cells originating from pluripotent mesenchymal stem cells. Mature human Chondrocytes are not in direct contact with BM in cartilage. However, several studies have reported the presence of individual BM components in adult cartilage matrix, such as laminin [19], perlecan [20], nidogen-2 [21] and collagen type IV [22]. Recently all four of these major BM components were reported together in pericellular cartilage matrix [23], which might indicate that chondrocytes are surrounded by the functional equivalent of a BM. Interestingly, these proteins are found in surrounding areas of cells in a similar arrangement to the BM in other tissues of mesenchymal origin, visualized by electron microscopy as thin electron dense structures underlying the cell layer (lamina densa). With progression of age this extensive ECM layer gradually becomes less and less distinct. In the cartilage of newborn mice, BMs are widespread in surrounding matrices, whereas in mature cartilage of adult mice BMs are localized mainly to a narrow pericellular zone [23]. However, prior to and during mesenchymal condensation and formation of the cartilagenous endplate, mesenchymal cells in the limb bud are embedded in ECM containing BM components, including laminin and type IV collagen, which could possibly influence differentiation of chondroprogenitor cells [24]. But there is a curious paucity of understanding of how the basement membrane directs cartilage development.

During embryonic development of cartilage initially all the scattered mesenchymal progenitor cells assume spread morphologies, but after few days they assume a rounded morphology and start to form aggregates [25]. These cell-cell homotypic interactions and cellular condensation play critical role to create a microenvironment which initiate chondrogenic differentiation during embryonic limb bud development. Limb bud initiation also requires reciprocal interactions between specialized ectoderm and progenitor cell. The chick limb bud model is the most commonly used model of in vivo limb chondrogenic pattern formation [26,27], involving the participation of various growth factors and morphogens such as fibroblast growth factor, hedgehog, wntless/Wnt, and bone morphogenetic proteins. Traditionally, chondrogenesis has also been studied in fixed and stained embryonic tissues using dyes and a limited set of molecular markers. Previous attempts to study the mesenchymal condensation stage of

chondrogenic development in vitro was carried out either by culturing chondrogenic cells in carboxymethyl cellulose [28], encapsulating the cells within alginate beads [29], or using cell pellets or micromass cultures [30,31]. For example, in the micromass system, limb mesenchyme dissociated into single cells, plated at high density, form cartilage nodules over 3-5 days in an attempt to recapitulate the formation and maturation of the cartilage endplate during embryonic skeletal development in vivo. None of these models address the role of the underlying BM morphology and mechanical compliance in mesenchymal condensation. However, to some extent the mechanochemical model [32] considers the interaction between cell migration and mechanical parameters of ECM in chondrogenic pattern formation. Attempts to disprove this model have been only partially successful [33]. It is still unclear whether a mechanochemical mechanism is responsible for the periodic nature of chondrogenic clustered pattern formation.

Therefore, in the present study, we aimed to investigate how nanofibrillar matrix architecture and stiffness affect gross cellular morphology of individual mesenchymal stem cells and in turn, can affect three dimensional organization at cellular level, govern chondrogenic differentiation with respect to matrix accumulation and gene expression. The goal was to clarify how matrix features may play a direct role in chondrogenesis by synergizing the impact of mechanical and morphological features in a single system.

2. Materials and Methods

2.1. Isolation of Silk fibroin

Aqueous silk fibroin solution was prepared by concentrating 8 wt% solution prepared as described previously [34]. In brief, cocoons of *B. mori* silkworm silk (Tajima Shoji Co., Ltd., Yokohama, Japan) were boiled for 30 min in an aqueous solution of 0.02 M Na₂CO₃, and then rinsed thoroughly with distilled water to extract the outer layer of glue-like sericin proteins of silk fibers. The extracted fibroin was dissolved in 9.3M LiBr solution at 60°C for 4 hr, yielding a 20 wt% aqueous solution. This solution was dialyzed against distilled water using Slide-a-Lyzer dialysis cassettes (MWCO 3,500, Pierce) at room temperature for 3 days to remove the salt. The dialysate was centrifuged twice, each at -5°C to 10°C for 20 min, to remove impurities and aggregates. The solution obtained from this process was approximately 8 wt%.

2.2. Electrospinning

7.5 wt% Silk/polyethylene oxide (PEO) solution, prepared by adding 5 ml of 5 weight % PEO (900,000 g/mol) into 20 ml of 8 wt% silk aqueous solution, was used to generate stable, continuous spinning [35]. Homogeneous solutions were obtained by stirring gently for at least 5 days at room temperature to avoid premature gelling. The solutions were filtered through a 5 mm syringe filter to remove remaining insoluble materials. Electrospinning was performed with a steel capillary tube with a 1.5 mm inside diameter tip mounted on an adjustable, electrically insulated stand as described earlier [35,36]. The capillary tube was maintained at a high electric potential for electrospinning and mounted in the parallel plate geometry. The capillary tube was connected to a syringe filled with silk/PEO spinning solution. Constant volume flow rate of 0.02 ml/min was maintained using a syringe pump. The voltage was kept constant at 13 kV and the distance between the capillary tube and the collection plate was varied (13 cm, 22 cm, 30 cm) to fabricate three different electrospun mats. As-spun nanofibrous mats were immersed into a 90/10 (v/v) methanol/water solution for 30 min and then immersed in distilled water for 24 hours to remove PEO, and finally dried at room temperature for 24 hr.

2.3. Atomic Force Microscopy

The elastic modulus of the silk nano-fibrillar architectures was evaluated using AFM (Multimode series, equipped with Nanoscope 4 controller, signal break-out box and vibration

detection electronics) attached to a digital oscilloscope and a data acquisition card (NI DAQ, S-series). The cantilever was excited to vibrate at its resonant frequency and was brought close to the sample. Intermittent contact with the surface alters the amplitude and phase of the cantilever vibration. The vibrations were detected with an optical system where a laser beam was reflected from the back of the cantilever and then dropped onto a position-sensitive photodetector. The set-point and free vibration amplitudes for the measurements were 40 nN and 60 nN. The drive frequency for the imaging was chosen to be slightly below resonance frequency. This favors repulsive-mode operation. Scan rate during the imaging was chosen to be 1 Hz. Next, the loading–unloading forces were observed and changes accurately with the time-resolved changes in compliance or stiffness of sample. These forces were used to estimate the stiffness of the nanofibre matrix surface and to calculate Lateral Modulus.

2.4. Cell culture

Human bone marrow derived mesenchymal stem cells (hMSCs) were suspended in 20 μ l chondrogenic media and statically seeded onto prewet nanofibrous matrix scaffolds (500,000 cells per scaffold, passage 2-3). Chondrogenic medium was DMEM supplemented with penicillin streptomycin, 100 nM dexamethasone, 50 mg/mL ascorbic acid-2-phosphate, insulin, transferrin, selenious acid premix (6.25 mg/mL bovine insulin, 6.25 mg/mL transferrin, 6.25 mg/mL selenious acid, 5.33 mg/mL linoleic acid, 1.25 mg/mL bovine serum albumin), 10 ng/mL TGF- β 1. The samples were cultured for up to 3 weeks at 37°C and 5% CO₂ with medium changed twice weekly. The whole cell culture process repeated to ensure reproducibility.

2.5. Scanning Electron Microscopy (SEM)

SEM images of the mats were taken with a Hitachi S-4700 SEM (Hitachi Ltd., Tokyo, Japan). Prior to imaging, samples were coated with gold for 45 sec (Emitech K575 Sputter Coater, Emitech Ltd., Ashford Kent, UK). For fibre diameter characterization, 30 diameter measurements were randomly recorded in each SEM image using the ‘Measure’ tool in ImageJ software (NIH, USA). Scaffolds seeded with hMSCs were fixed at different time points in PBS containing 2.5% glutaraldehyde for 1 hr at room temp, rinsed in PBS, and dehydrated in increasing concentrations of ethanol (25%, 50%, 60%, 80%, 100%) and air dried. After drying, they were sputter-coated with gold and viewed with a voltage of 10 kV under low vacuum.

2.6. Real-time Polymerase chain reaction (RT-PCR)

Total RNA was extracted from seeded scaffolds following 21 days of cultures using RLT buffer (Qiagen RNeasy kit). cDNA were synthesized using high-capacity cDNA Archive kit (ABI Biosystems) following the manufacturer's instructions. The PCR master mix was based on AmpliTaq Gold DNA polymerase (Applied Biosystems). cDNA samples were analyzed for the gene of interest and the housekeeping gene in independent reactions using commercially available primers and probes from Assays-on-Demand™ Gene Expression kits (FN1, Product # Hs00365052_m1; Integrin alpha 5 (fibronectin receptor), Product # Hs00233732_m1; AGC1, Product # Hs00202971_m1; ITGAV, Product # Hs 00233808_m1; Sox-9, Product # Hs00165814_m1; Collagen type II, Product # Hs00264051_m1; Integrin beta 1 (fibronectin receptor, beta polypeptide), Product # Hs00236976_m1; Ras homolog gene family, member A, (RhoA) Product # Hs00236938_m1; CDC42, Product # Hs00918044_g1) following the manufacturer's instructions while the housekeeping gene GAPDH was analyzed using primers and probes. Data analysis was performed using the ABI Prism 7000 Sequence Detection Systems version 1.0 software (Applied Biosystems, Foster City, CA). For each cDNA sample, the Ct value was defined as the cycle number at which the fluorescence intensity reached 0.45 at which amplification of each target gene was within the linear range of the reaction. Relative expression levels for each gene of interest were calculated by normalizing the quantified cDNA

transcript level (Ct) to the GAPDH ($2^{\Delta Ct}$ formula, Perkin Elmer User Bulletin #2). Each cDNA sample was assessed at least in duplicate.

2.7. Histology

Following 3 weeks of static culture, scaffolds were fixed in 2.5 % formalin for 24 h at 4°C. Scaffolds were then embedded in optimal cutting temperature (OCT) tissue freezing mixture and 5 µm sections were cut and subsequently stained with Alcian blue. The slides were mounted with glycerol gelatin, and at least three surface sections per scaffold were examined with a Zeiss Axiovert S100 light microscope.

2.8. Staining of the beta-actin cytoskeleton for immunofluorescence

Cells were seeded on the silk mats and kept in culture for up to 3 weeks. To visualize the cytoskeleton, the cells were rinsed in PBS, fixed with 4% paraformaldehyde in PBS for 30 min, permeabilized with 0.1% Triton-X100, and stained with anti-vinculin-FITC conjugate antibody and rhodamine-conjugated phalloidin (Sigma) for 30 min at 4°C. The samples were investigated by a confocal laser scanning microscope (Leica, DMIRE2).

2.9. Biochemical Analysis

For determination of GAG and DNA, constructs were collected at each time point, washed with PBS, weighed and digested with proteinase K (1 mg/mL protease K in 50 mmol/L Tris with 1 mmol/L EDTA, 1 mmol/L iodoacetamide, and 10 µg/mL pepstatin-A) for 15 hours at 56°C. GAG content was measured spectrophotometrically using dimethylmethylene blue dye, with chondroitin sulfate as a standard. The GAG content was normalized to the amount of DNA, which was measured using a CyQUANT cell proliferation assay kit (Molecular Probes) with calf thymus DNA as a standard.

2.10. TEM

Samples were fixed in 2.5% glutaraldehyde in 0.1 M sodium cacodylate buffer, pH 7.3, at 37°C, then stored at 4°C. They were rinsed in buffer, post-fixed in 1% osmium tetroxide, rinsed in buffer, dehydrated in graded alcohols and propylene oxide, and embedded in epon 812 resin. Sections were cut to 70-90 nm on a diamond knife on a Reichert-Jung ultracut microtome, stained with 2% uranyl acetate, and viewed with a Philips CM-10 electron microscope at 80 KV.

3. Results

3.1. Characterization of nanofibrous matrixes

The electrospinning process was carried out with 8% aqueous silk fibroin solution with PEO to develop adequate viscosity and surface tension [36]. Three electrospun nanofibrous mats were formed by varying the spinning distance (13 cm, 22 cm and 30 cm), with the three choices selected based on feasibility limits. Fibers could not evaporate solvent when the distance between capillary and collecting plate was less than 13 cm, as evidenced by the accumulation of silk solution on collecting plate. Beyond 30 cm distance from spinneret, the electrostatic attraction became so weak that continuous fibre deposition was disrupted. An intermediate point (22 cm) was selected between these two extreme points.

Nanofibre diameter distributions analyzed by using SEM images revealed narrowing of fibre diameter distribution with increasing distance. SEM images (Figure 1) demonstrated that the nanofibers produced were straight, with stretched morphologies when the distance between spinneret and collecting plate was 13 cm. As the distance between spinneret and collecting plate increased, the fibers gradually assumed relaxed and loopy morphologies. The longer the

flight length, the longer time to remove the solvent; hence drier fibres, with enhanced molecular orientation suggestive of different stiffness in the different nanofibrous mats. In order to evaluate the differences in matrix stiffness AFM studies were conducted (Figure 2). Time resolved forces were determined on each point (pixel) formed due to the interaction of cantilever tip and fibrous matrix interaction, when the tip of the cantilever was in tapping mode. This method is non-destructive and thus preferred vs. destructive methods such as nano-indentation, as we conducted earlier [37]. Previously using nanoindentation technique, we have demonstrated that after methanol treatment and extraction with water, the electrospun silk fiber exhibits a lateral modulus of about 8 GPa. Using tapping mode cantilever, a certain force (set point, 40 nN) was constantly applied and changes in peak forces were noticed. Then the time-resolved forces were used to calculate lateral modulus at each point of interaction over a fixed selected length. The data indicated that the nanofibres of the 30 cm mat (4.8 ± 0.37 GPa) had significantly lower stiffness when compared to that of the 13 cm mat (7.8 ± 0.54 GPa), whereas 22 cm mat had intermediate modulus (6.1 ± 0.42 GPa). This difference was most likely due to enhancement in molecular orientation and crystallinity content, as proposed earlier [37]. Another interesting observation of AFM study (Figure 2) was at 30 cm mat, nanofibres were loosely deposited over underlying fibrous layers, and as the cantilever tip moved, fibres showed flexibility to move, whereas at 13 and 22 cm mats, nanofibres were attached with underlying layers, which can in turn give rise to enhanced rigidity of matrix.

3.2. Modulation of cell spreading due to matrix stiffness

Silk fibroin is a naturally occurring degradable fibrous protein, made up of mostly amino acids like glycine, alanine, serine, tyrosine. When bone marrow-derived mesenchymal stem cells were cultured on the 13 cm mat (stiffest matrix with stretched nanofibres), cells continued to grow maintaining a spread morphology (Figure 3). Interestingly, on the 30 cm matrix (malleable nanofibrous matrix) cells initially assumed a spread morphology but after 3-4 days started to assume a rounded morphology. After 8-10 days of culture in the presence of chondrogenic media, cells migrated and formed aggregates on the 30 cm mats. Few cells found to be still in spindle shape and radially orientated toward the center of the aggregates, suggesting high cell motility over flexible nanofibrous matrix. This spontaneous response, cued only in part by chondrogenic factors as this did not occur on the other mats, mimics to some extent the 'mesenchymal condensation' step, which is a pre-requisite in the process of chondrogenesis. After 15 days these precartilaginous aggregates stabilized and contour of clusters gradually became oblong to roundish, whereas the outside boundary was still uneven with some cells extending filopodia anchoring nearby nanofibres. Around 18-20 days cell layers at the peripheral edge of clusters became elongated, circumfering the perimeter of the condensation; thus probably developing the putative 'perichondrium'-like tissue. This led to the smooth and more organized appearance of the precartilaginous condensations, resulting in firm, compact cartilage nodules.

To examine how the nanofibrous architecture and compliance affected cell morphology, cytoskeletal organization of the hMSCs was stained with rhodamine-phalloidin, and FITC-vinculin. After 10 days of culture, on the 13 cm matrix large, long, parallel actin stress fibers were noticed inside the spindle-shaped cells, confirming the rigidity of the underlying matrix, whereas on the 30 cm mats short punctate actin staining was uniformly scattered in the cytoplasm (Figure 4). Vinculin was uniformly distributed throughout the cells on the stiffer mats at the contact points between the cells and the nano-fibers. In contrast, on the softer mats vinculin accumulated in a disorganized fashion mostly on the peripheral parts of the cells, which in turn indicates chondrogenic differentiation [34]. These observations indicate that difference in cytoskeletal organization of hMSCs cultured on the different nanofibrillar scaffolds can induce modulation in differentiation potential.

3.3. Modulation of chondrogenic gene expression

To gain further insight into chondrogenic differentiation on the different mats with different stiffness, the role of stem cell morphology with chondrogenic matrix production was assessed. After 4 weeks of culture (Figure 5A), cells cultured on the relaxed matrix (30 cm mat) produced significantly more glucosaminoglycan (normalized to DNA content) and expressed a higher mRNA content of collagen type II, compared to the stiffer matrices (13 and 22 cm mats). Alcian blue staining (Figure 5B) further confirmed difference in staining intensity and modulation of cell morphology from stiff to comparatively flexible matrixes.

It will be intriguing to understand how cellular signaling mechanisms are gradually controlled by the compliance of the extracellular matrix to govern kinetics of stem cell differentiation and how it acts synergistically with chondrogenic soluble factors. Expression level of transcript for Aggrecan was significantly higher from the 30 cm mat, compared to the other two stiffer matrices; and even within the 30 cm mat transcript levels increased with cultivation time (Figure 6). The SOX9 transcription factor is an early marker of chondrogenic differentiation. During embryonic development *in vivo* Sox9 is broadly expressed prior to initiation of limb mesenchymal condensations, followed by the expression of definitive cartilage markers such as collagen type IIa [38,39]. Cells grown over 30 cm mat maintained higher level of Sox-9 expression after 2 weeks. Transcripts encoding Rho-A was strongly upregulated in rigid mat, compared to flexible 30 cm mat, which again supported enhanced spreading at stiffer mats. hMSCs cultured over flexible matrix showed continual enhancement in Fibronectin mRNA expression, indicating that three weeks of culture was insufficient to achieve full extent of chondrogenic differentiation [40]. Level of mRNA expression of CDC42 (cell Division cycle 42), a small GTPase of the Rho-subfamily, sharply enhanced around 3 weeks on 30 cm mat, compared to stiffer mats. Expression of integrin $\alpha\beta 5$, which is vitronectin/osteopontin receptors, was not significantly modulated on different nanofibrous mats.

3.4. Organization of hMSCs and hESCs during chondrogenic differentiation

TEM studies have been done to understand how hMSCs are committed to chondrogenic pathways over flexible nanofibrous mat with time. At day 5, when cells started to form aggregates, TEM images (Figure 7A) of hMSC aggregates showed a uniform presence of gap junctions and tight junctions. The presence of rough endoplasmic reticulum may indicate the synthesis and secretion of extracellular matrix proteins. Interestingly after 10 days, the cell-cell homotypic junctions disassembled by filling the intercellular space with ECM (Figure 7B). Faint fibrous depositions and electron-dense proteoglycan molecules were also observed. After 20 days, enhancement of pericellular matrix, especially with abundant collagen fibers was seen; collagen type II is putatively evident by the segments (Figure 7C) [41]. Interestingly, a high content of lipid vacuoles in the cytoplasm of the cells was observed only on cell aggregates formed on 30 cm mat, as previously reported in pellet culture of redifferentiated stem cells [42].

Most of studies for understanding underlying mechanisms of mesenchymal condensation have been performed using micromass culture with embryonic limb bud cells. Evidence of mesenchymal aggregation on silk nanofibrous mats, in presence of chondrogenic soluble factors, stimulated efforts to explore the response of human embryonic stem cells (ES) on nanofibrous mats with different mechanical flexibilities. As H9 ES cells (passage 35) were seeded on the 30 cm mat in aggregated form, thus no significant modulation in cell migration or aggregate size was noticed over 10 days of culture. TEM images of the ES cell clusters showed that initially all the ES cells were in close contact with each other, maintaining a rounded cell shape typical of ES cells (Figure 8A, 8B). After 10 days within the aggregates individual cells were separated by putative ECM, which may be simulating “chondron”-like morphology. The prominent presence of lipid vacuoles in the cytoplasm was also noticed in

the ES aggregates (Figure 8D), as reported earlier for chondrogenic differentiation of mouse ES cells [43].

4. Discussion

A main challenge in the field of tissue engineering is to recapitulate native developmental processes, which take place *in vivo* generally for years, into a compressed time frame within *in vitro* tissue culture. This is the first report to establish a simple *in vitro* model of such processing to understand mechanisms of mesenchymal condensation during chondrogenic development. Engler et al [14] elegantly reported lineage-specific differentiation of mesenchymal stem cells as function of modulation in stiffness of two-dimensional matrix based on polyacrylamide gels coated with collagen. However three-dimensional nanofibrillar matrix with suitable compliance would be pertinent to mimic the *in vivo* tissue microenvironment. Fiber diameter, structure and physical properties of the nanofiber matrices were tuned by controlling the spinning distance and the effective applied field strength during electrospinning process. AFM studies confirmed that by increasing the distance between spinneret and collecting plate during electrospinning a nanofibrillar matrix with reduced stiffness and enhanced flexibility can be fabricated, which can match the compliance of neonatal and adult basement membranes in animal model [44,45].

Several studies have reported chondrogenic differentiation of hMSCs on electrospun nanofibrous mats [46]. In all these studies, cells grew with spread morphologies as in monolayer cultures. In the present work, we report for the first time the aggregation of hMSCs on electrospun nanofibrous mats, depending upon the relative stiffness of the matrix, which would lead to 3D tissues, and thus more physiologically relevant systems. Cells sense subtle variation in nano-fibrillar matrix stiffness and topographies. Stiffer underlying matrix can resist cell-generated traction force. This response eventually modulates cell functions. In the relaxed matrix, where nanofibres are loosely deposited over each other, cells could easily distort fibers to migrate and assume rounded and aggregated morphologies, stimulating chondrogenesis mechanisms. We can not exclude the possibility that cellular migration might be governed by matrix stiffness or matrix topography, local gradients of deposited ECM, or soluble factors, or combinations of some of these issues. However the identification of factors influencing cellular motility in 3D matrices have already been elucidated [47], leading to concepts in scaffold fabrication. Maximal cell movement occurs in matrices exhibiting lower stiffness [48], which has been directly confirmed by our study.

The level of chondrogenesis regulating transcripts, such as collagen-II, Sox-9, aggrecan and fibronectin were significantly lower in nanofibrillar matrices with higher stiffness, where cells maintained their spread morphology and hence, poor tissue forming ability, compared to the cells grown on nanofibrillar matrices with relatively reduced stiffness. Sox9 has an essential role in early stage chondrogenic differentiation. Sox9-null cells fail to differentiate into chondrocytes. Sox9 regulates the transcription of cartilage-specific ECM molecules. One of the earliest direct transcription targets and effectors of Sox9 activity is Collagen type IIa, which is a definitive marker of chondrogenic differentiation [49]. Previously reported *in vivo* results suggest that the chondrogenic soluble factors (such as, TGF- β family) induce cellular aggregation by upregulating adhesive glycoprotein fibronectin [50]. Cells first form aggregates in the region of cell-fibronectin interaction points [51,52], followed by cell differentiation follows at that site of condensation [53]. Our results address such type of intracellular signaling cascades involved during mesenchymal condensation steps of chondrogenic development, in cue of nanofibrillar matrix morphology and stiffness.

Integrin-mediated signaling plays crucial role in generation and maintenance of chondrocytic phenotype during chondrogenic differentiation. Particularly, the receptors for fibronectin,

vitronectin, osteopontin and collagens may be involved in cartilage-specific ECM generation. Integrins $\alpha_1\beta_1$, $\alpha_5\beta_1$, $\alpha_6\beta_1$, and $\alpha_v\beta_5$ are commonly reported in intact cartilage, but $\alpha_5\beta_1$, the classical fibronectin receptor, is reported to be the most abundant of the β_1 -containing integrins in fetal cartilage [54], controlling chondrocyte survival, function and mechanotransduction, by acting as a mechanoreceptor [55]. During early chondrogenesis, fibronectin is reported to upregulate integrin expression on the surface of undifferentiated chondroprogenitors to enhance cell-cell interactions, condensation and expression of chondrogenic differentiation markers. In this in vitro model system, expression of mRNA encoding β_1 -integrin was significantly upregulated in hMSCs cultured over flexible mats, synchronized with fibronectin mRNA expression kinetics. Ras homolog gene family, member A (RhoA), a small GTPase, is responsible for integrating mechanical signals from the ECM to the cell, and its activation enhances cell-generated tractional forces in monolayer cultures on stiffer surfaces by expressing actin stress fibers and focal adhesions [56]. In our in vitro model hMSCs cultured over stiffer mats showed stress fibers, and their RhoA expression level was comparatively higher than on the more flexible mats. It is known that RhoA acting through Rho kinase (ROCK) promotes the formation of stress fibers and spread-shaped cells [57]. Interestingly, unlike RhoA, expression of Cdc42 RhoGTPase transcript was upregulated in cells grown over 30 cm mat during cell aggregation stage, indicating potential role of cdc42 in cell aggregation process.

Cellular contact and gap junction-mediated intercellular coupling play crucial roles in mesenchymal condensation during early chondrogenesis [58,59]. In studies based on micromass cultures of mouse limb buds and/or chick wing buds, cells at the periphery flatten, while central cells maintain a round cell morphology associated with early differentiation into cartilage, as seen by live time-lapse imaging system to visualize the dynamics of limb mesenchyme undergoing chondrogenesis [60]. Most interestingly, in the present study, both hMSCs and ES cells demonstrated very similar phenomenon of initial homophilic cell-cell contact formation, as an initiating step in chondrogenesis, which were gradually separated by cartilage-specific matrix depending on subtle variation of stiffness of the underlying nanofibrillar mats. On distortable, relaxed nanofibrillar matrices, in vitro, cells behaved very similar to that which has been reported previously during early chondrogenesis in in vivo embryo limb bud models [58,59], demonstrating gradual morphological changes associated with early chondrogenic differentiation.

5. Conclusions

The intertwinement of nanofibrous scaffold matrix compliance, cell shape, cytoskeletal mechanics, and developmental processes was been addressed by simulating nanofibrillar matrix morphology in the basement membranes. Insight into how polymeric scaffold matrix compliance guides chondrogenic tissue regeneration was obtained with both human embryonic stem cells and adult stem cells in the presence of chondrogenic soluble factors. This relatively simple nanofiber matrix-based in vitro system allows the study of 3D chondrogenic development.

Acknowledgments

We thank the NIH Tissue Engineering Resource Center (EB002520) for support of this research.

References

1. Lysaght MJ, Hazlehurst AL. Tissue engineering: the end of the beginning. *Tissue Eng* 2004;10:309–20. [PubMed: 15009955]

2. Fischbach C, Chen R, Matsumoto T, Schmelzle T, Brugge JC, Polverini PJ, et al. Engineering tumors with 3D scaffolds. *Nature Methods* 2007;4:855–60. [PubMed: 17767164]
3. Ghosh, S.; Kaplan, DL. In Vitro 3D Human Tissue Models for Osteochondral Diseases. In: Polak, L., editor. *Advances in Tissue Engineering*. Imperial College Press; UK: 2008. p. 781-805.
4. Rosowski M, Falb M, Tschirschmann M, Lauster R. Initiation of Mesenchymal Condensation in Alginate Hollow Spheres—A Useful Model for Understanding Cartilage Repair? *Artificial Organs* 2006;30:775–84. [PubMed: 17026577]
5. Mondrinos MJ, Koutzaki S, Lelkes PI, Finck CM. A tissue-engineered model of fetal distal lung tissue. *Am J Physiol- Lung Cell Mol Physiol* 2007;293:L639–L650. [PubMed: 17526596]
6. Nesbitt TL, Patel PA, Yost MJ, Goodwin RL, Potts JD. A 3-D model of coronary vessel development. *In Vitro Cell Dev Biol – Animal* 2007;43:10–16.
7. Clark CC, Tolin BS, Brighton CT. The effect of oxygen tension on proteoglycan synthesis and aggregation in mammalian growth plate chondrocyte. *J Orthop Res* 1991;9:477–84. [PubMed: 2045974]
8. Wang Y, Blasioli DJ, Kim HJ, Kim HS, Kaplan DL. Cartilage tissue engineering with silk scaffolds and human articular chondrocytes. *Biomaterials* 2006;27:4434–442. [PubMed: 16677707]
9. Zanetti NC, Solorsh M. Induction of chondrogenesis in limb mesenchymal cultures by disruption of the actin cytoskeleton. *J Cell Biol* 1984;99:115–23. [PubMed: 6539780]
10. Brown PD, Benya PD. Alterations in chondrocyte cytoskeletal architecture during phenotypic modulation by retinoic acid and dihydrocytochalasin B-induced reexpression. *J Cell Biol* 1988;106:171–79. [PubMed: 3276712]
11. Mallein-Gerin F, Garrone R, Van der Rest M. Proteoglycan and collagen synthesis are correlated with actin organisation in dedifferentiating chondrocytes. *Eur J Cell Biol* 1991;56:364–73. [PubMed: 1802719]
12. Motta C, Fodor J, Sziogyarto Z, Juhasz T, Gergely P, Csernoch L, et al. Cytosolic free Ca(2+) concentration exhibits a characteristic temporal pattern during in vitro cartilage differentiation: A possible regulatory role of calcineurin in Ca-signalling of chondrogenic cells. *Cell Calcium* 2008;44:310–23. [PubMed: 18291522]
13. Jakob M, Demartean O, Schafer D, Hintermann B, Dick W, Heberer M, et al. Specific growth factors during the expansion and redifferentiation of adult human articular chondrocytes enhance chondrogenesis and cartilaginous tissue formation in vitro. *J Cell Biochem* 2001;81:368–77. [PubMed: 11241676]
14. Engler AJ, Sen S, Sweeney HL, Discher DE. Matrix elasticity directs stem cell lineage specification. *Cell* 2006;126:677–89. [PubMed: 16923388]
15. Peyton SR, Ghajar CM, Khatiwala CB, Putnam AJ. The emergence of ECM mechanics and cytoskeletal tension as important regulators of cell function. *Cell Biochem Biophys* 2007;47:300–20. [PubMed: 17652777]
16. Lutolf MP, Hubbell JA. Synthetic biomaterials as instructive extracellular microenvironments for morphogenesis in tissue engineering. *Nat Biotechnol* 2005;23:47–55. [PubMed: 15637621]
17. Ghosh K, Pan Z, Guan E, Ge S, Liu Y, Nakamura T, et al. Cell adaptation to a physiologically relevant ECM mimic with different viscoelastic properties. *Biomaterials* 2007;28:671–79. [PubMed: 17049594]
18. Ghosh K, Ingber D. Micromechanical control of cell and tissue development: implications for tissue engineering. *Adv Drug Deliv Rev* 2007;59:1306–318. [PubMed: 17920155]
19. Lee SK, Malpeli M, Cancedda R, Utani A, Yamada Y, Kleinman HK. Laminin chain expression by chick chondrocytes and mouse cartilaginous tissues in vitro and in vivo. *Exp Cell Res* 1997;236:212–22. [PubMed: 9344601]
20. French MM, Smith E, Akanbi T, Sanford T, Hecht J, Farach-Carson MC, et al. Expression of the heparin sulfate proteoglycan, perlecan, during mouse embryogenesis and perlecan chondrogenic activity in vitro. *J Cell Biol* 1999;145:1103–115. [PubMed: 10352025]
21. Salmivirta K, Talts JF, Olsson M, Sasaki T, Timpl T, Ekblom P. Binding of mouse nidogen-2 to basement membrane components and cells and its expression in embryogenic and adult tissue suggest complementary functions of the two nidogens. *Exp Cell Res* 2002;279:188–201. [PubMed: 12243745]

22. SundarRaj N, Fite D, Ledbetter S, Chakravarti S, Hassell JR. Perlecan is a component of cartilage matrix and promotes chondrocyte attachment. *J Cell Sci* 1995;108:2663–672. [PubMed: 7593307]
23. Kvist AJ, Nystrom A, Hultenby K, Sasaki K, Talts JF, Aspberg A. The major basement membrane components localize to the chondrocytes pericellular matrix- A cartilage basement membrane equivalent? *Matrix Biol* 2007;27:22–33. [PubMed: 17825545]
24. Solorsh M, Jensen KL. The accumulation of basement membrane components during the onset of chondrogenesis and myogenesis in the chick wing bud. *Development* 1988;104:41–49. [PubMed: 3253060]
25. Stott NS, Jiang TX, Choung C. Successive Formative Stages of Precartilaginous Mesenchymal Condensations In Vitro: Modulation of Cell Adhesion by Wnt-7A and BMP-2. *J Cell Physiol* 1999;180:314–324. [PubMed: 10430171]
26. Niswander L. Pattern formation: old models out on a limb. *Nat Rev Genet* 2003;4:133–43. [PubMed: 12560810]
27. Tickle C. Patterning systems--from one end of the limb to the other. *Dev Cell* 2003;4:449–58. [PubMed: 12689585]
28. Tacchetti C, Tavella S, Dozin B, Quarto R, Robino G, Cancedda R. Cell condensation in chondrogenic differentiation. *Exp Cell Res* 1992;200:26–33. [PubMed: 1563490]
29. Rosowski M, Falb M, Tschirschmann M, Lauster R. Initiation of Mesenchymal Condensation in Alginate Hollow Spheres—A Useful Model for Understanding Cartilage Repair? *Artif Organs* 2006;30:775–84. [PubMed: 17026577]
30. Ichinose S, Tagami M, Muneta T, Sekiya I. Morphological examination during in vitro cartilage formation by human mesenchymal stem cells. *Cell Tissue Res* 2005;322:217–26. [PubMed: 16091918]
31. Daniels K, Reiter R, Solorsh M. Micromass cultures of limb and other mesenchyme. *Methods Cell Biol* 1996;51:237–47. [PubMed: 8722479]
32. Oster GF, Murraray JD, Harris AK. Mechanical aspects of mesenchymal morphogenesis. *J Embryol Exp Morphol* 1983;78:83–125. [PubMed: 6663234]
33. Wolpert L, Hornbruch A. Double anterior chick limb buds and models for cartilage rudiment specification. *Development* 1990;109:961–66. [PubMed: 2226209]
34. Ghosh S, Parker ST, Wang X, Kaplan DL, Lewis JA. Direct-Write Assembly of Micro-Periodic Silk Fibroin Scaffolds for Tissue Engineering Applications. *Adv Func Mater* 2008;18:1883–89.
35. Li C, Vepari C, Jin HJ, Kim HJ, Kaplan DL. Electrospun silk-BMP-2 scaffolds for bone tissue engineering. *Biomaterials* 2006;27:3115–24. [PubMed: 16458961]
36. Jin HJ, Fridrikh SV, Rutledge GC, Kaplan DL. Electrospinning Bombyx mori silk with poly(ethylene oxide). *Biomacromolecules* 2002;3:1233–39. [PubMed: 12425660]
37. Wang M, Jin HJ, Kaplan DL, Rutledge GC. Mechanical Properties of Electrospun Silk Fibers. *Macromolecules* 2004;37:6856–64.
38. Akiyama H, Chaboissier MC, Martin JF, Schedl A, de Crombrugge B. The transcription factor Sox9 has essential roles in successive steps of the chondrocyte differentiation pathway and is required for expression of Sox5 and Sox6. *Genes Dev* 2002;6:2813–28. [PubMed: 12414734]
39. Wright E, Hargrave MR, Christiansen J, Cooper L, Kun J, Evans T, et al. The Sry-related gene Sox9 is expressed during chondrogenesis in mouse embryos. *Nature Genet* 1995;9:15–20. [PubMed: 7704017]
40. Kulyk W, Upholt WB, Kosher RA. Fibronectin gene expression during limb cartilage differentiation. *Development* 1989;106:449–55. [PubMed: 2598818]
41. Holmes DF, Graham HK, Trotter JA, Kadler KE. STEM/TEM studies of collagen fibril assembly. *Micron* 2001;32:273–85. [PubMed: 11006507]
42. Yang KG, Saris DB, Geuze RE, Helm YJ, Rijen MH, Verbout AJ, et al. Impact of expansion and redifferentiation conditions on chondrogenic capacity of cultured chondrocytes. *Tissue Eng* 2006;12:2435–47. [PubMed: 16995777]
43. Kramer J, Klinger M, Kruse C, Faza M, Hargus G, Rohwedel J. Ultrastructural analysis of mouse embryonic stem cell-derived chondrocytes. *Anat Embryol* 2005;210:175–85. [PubMed: 16211392]

44. Candiello J, Balasubramani M, Schreiber EM, Cole GJ, Mayer U, Halfter W, et al. Biomechanical properties of native basement membranes. *FEBS J* 2007;274:2897–908. [PubMed: 17488283]
45. Welling LW, Zupka MT, Welling DJ. Mechanical Properties of Basement Membrane. *News Physiol Sci* 1995;10:30–35.
46. Li WJ, Jiang YJ, Tuan RS. Chondrocyte phenotype in engineered fibrous matrix is regulated by fiber size. *Tissue Eng* 2006;12:1775–85. [PubMed: 16889508]
47. Hartmann A, Boukamp P, Friedl P. Confocal reflection imaging of 3D fibrin polymers. *Blood Cells Mol Dis* 2006;36:191–93. [PubMed: 16488165]
48. Zaman MH, Trapani LM, Siemeski A, MacKellar D, Gong HY, Kamm RD, et al. Migration of tumor cells in 3D matrices is governed by matrix stiffness along with cell-matrix adhesion and proteolysis. *Proc Natl Acad Sci USA* 2006;103:10889–894. [PubMed: 16832052]
49. Lefebvre V, Huang W, Harley VR, Goodfellow PN, de Crombrughe B. Sox9 is required for cartilage formation. *Mol Cell Biol* 1997;17:2336–46. [PubMed: 9121483]
50. Miura T, Shiota K. TGF- β 2 acts as an ‘activator’ molecule in reaction-diffusion model and is involved in cell sorting phenomenon in mouse limb micromass culture. *Dev Dyn* 2000;217:241–49. [PubMed: 10741418]
51. Frenz DA, Jaikaria NS, Newman SA. The mechanism of precartilaginous mesenchymal condensation: a major role for interaction of the cell surface with the amino-terminal heparin-binding domain of fibronectin. *Dev Biol* 1989;136:97–103. [PubMed: 2806726]
52. Widelitz RB, Jiang TX. Adhesion molecules in skeletogenesis: II. Neural cell adhesion molecules mediate precartilaginous mesenchymal condensations and enhance chondrogenesis. *J Cell Physiol* 1993;156:399–411. [PubMed: 8344994]
53. Hall BK, Miyake T. All for one and one for all. *Bioessays* 2000;22:138–47. [PubMed: 10655033]
54. Häusler G, Helmreich M, Marlovits S, Egerbacher M. Integrins and extracellular matrix proteins in the human childhood and adolescent growth plate. *Calcif Tissue Int* 2002;71:212–18. [PubMed: 12154393]
55. Wright MO, Nishida K, Bavington C, Godolphin JL, Dunne E, Walmsley S, et al. Hyperpolarisation of cultured human chondrocytes following cyclical pressure-induced strain: evidence of a role for alpha 5 beta 1 integrin as a chondrocyte mechanoreceptor. *J Orthop Res* 1997;15:742–47. [PubMed: 9420605]
56. Hall A. Rho GTPases and the actin cytoskeleton. *Science* 1998;279:509–14. [PubMed: 9438836]
57. McBeath R, Pirone DM, Nelson CM, Bhadriraju K, Chen CS. Cell shape, cytoskeletal tension, and RhoA regulate stem cell lineage commitment. *Dev Cell* 2004;6:483–95. [PubMed: 15068789]
58. Coelho CN, Kosher RA. Gap junctional communication of cartilage: in vitro evaluation. *Dev Biol* 1991;144:47–53. [PubMed: 1995401]
59. Zimmermann B. Assembly and disassembly of gap junctions during mesenchymal cell condensation and early chondrogenesis in limb bud of mouse embryo. *J Anat* 1984;138:351–63. [PubMed: 6715255]
60. Barna M, Niswander L. Visualization of Cartilage Formation: Insight into Cellular Properties of Skeletal Progenitors and Chondrodysplasia Syndromes. *Develop Cell* 2007;12:931–41.

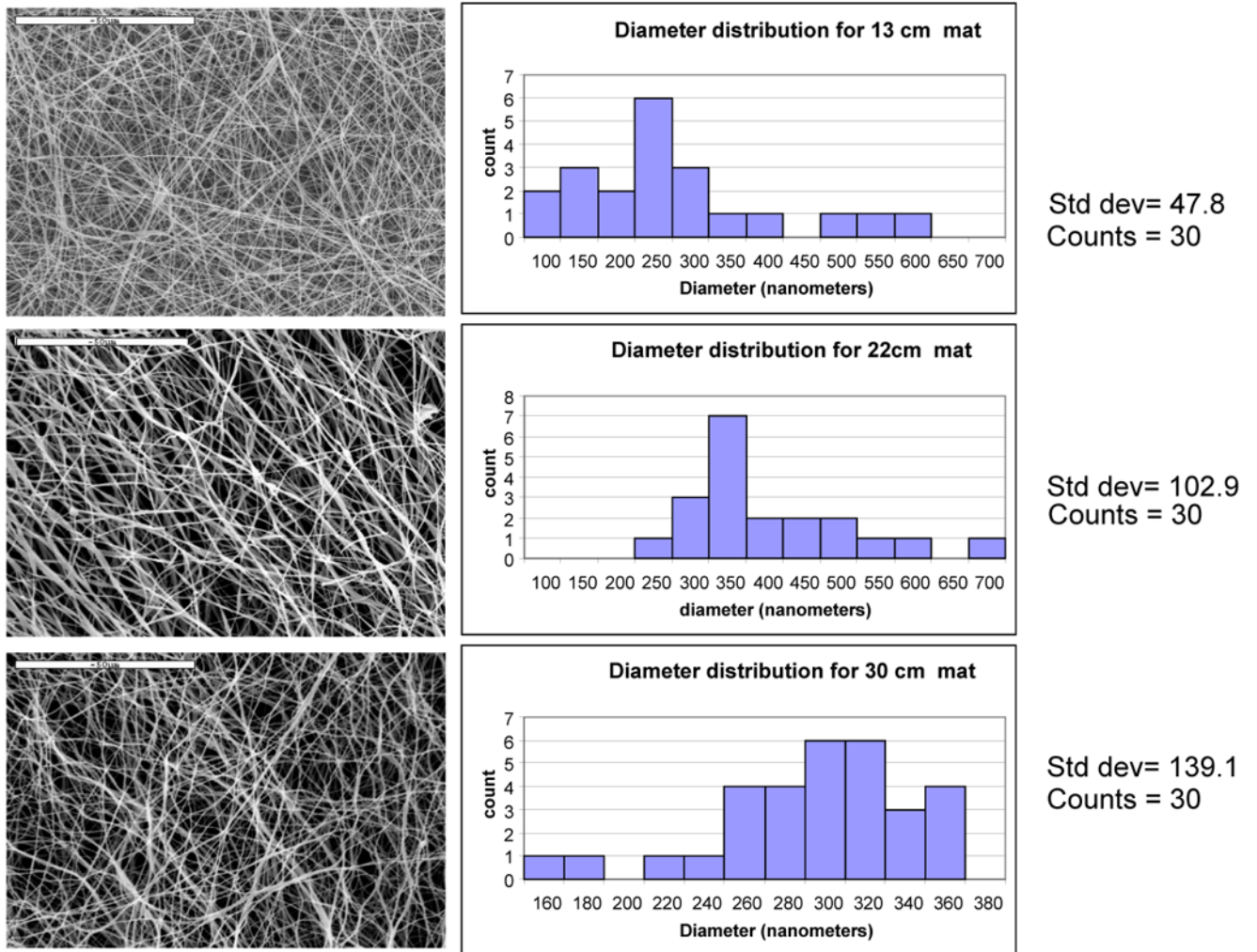


Figure 1.
Characterization of fiber diameter distribution: A: 13 cm mat, B: 22 cm mat, C: 30 cm mat

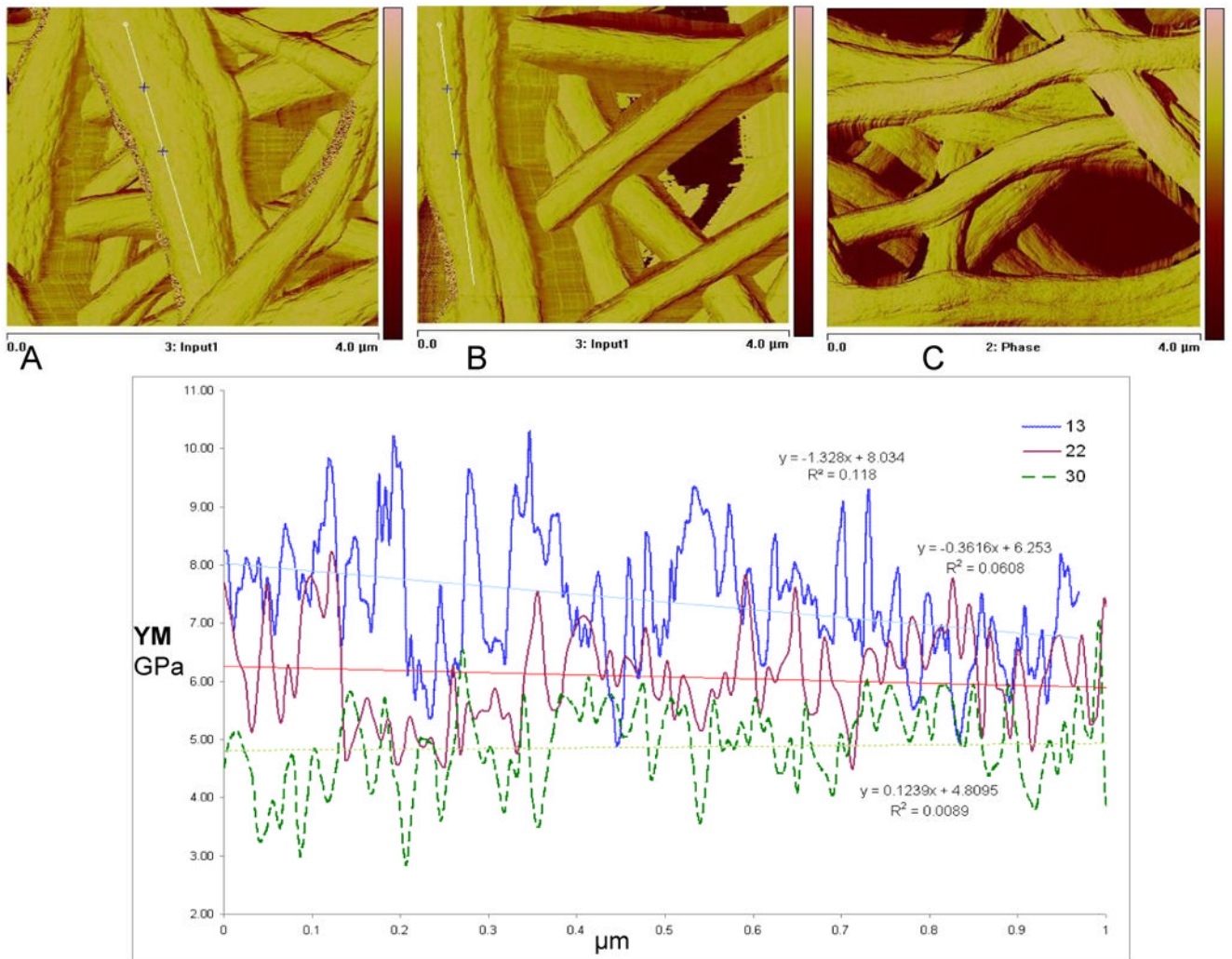


Figure 2. Measurement of nanofiber modulus by AFM: A: 13 cm mat, B: 22 cm mat, C: 30 cm mat

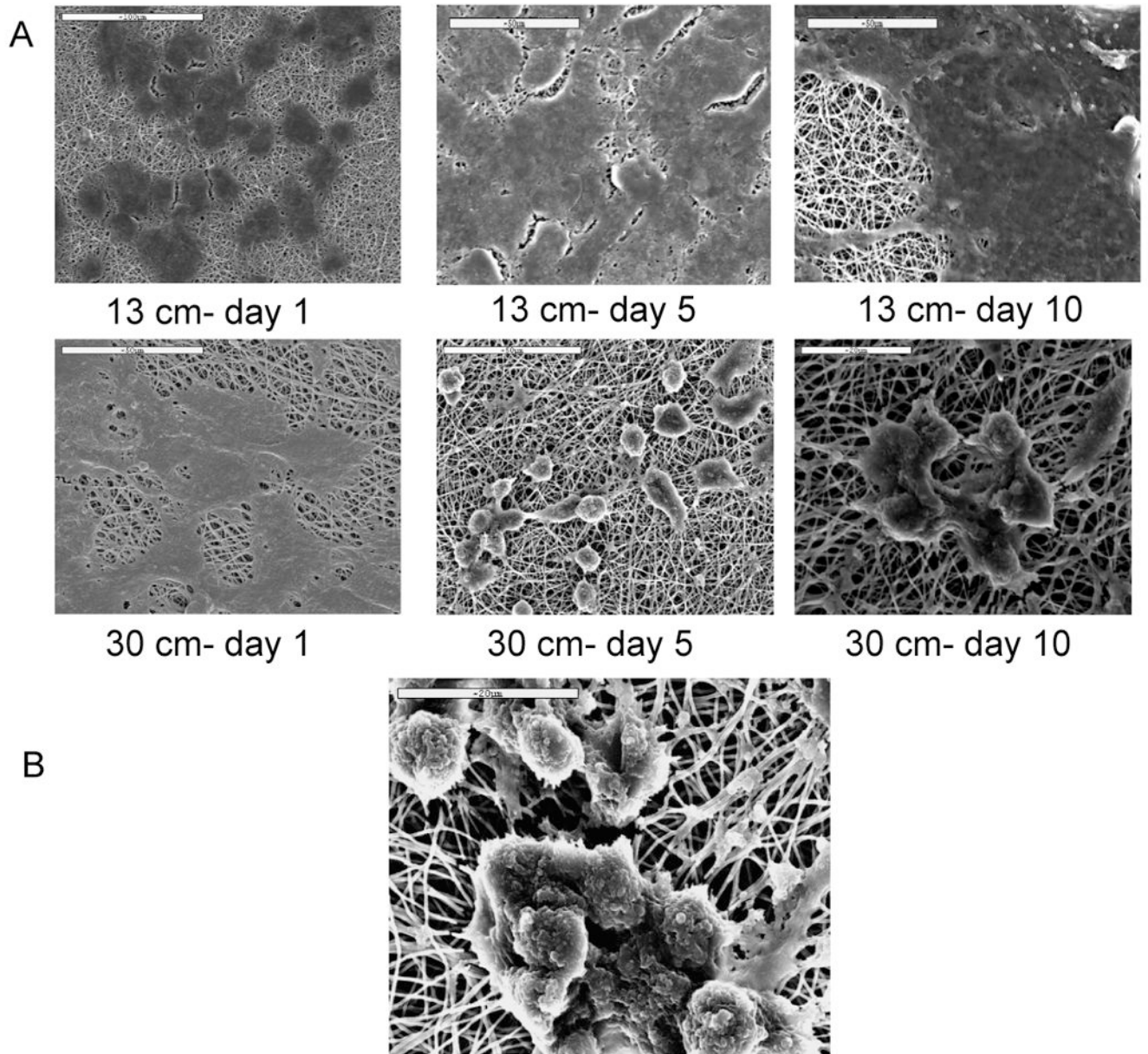


Figure 3. Modulation of cell morphology in signal of subtle variation in matrix stiffness, (i) hMSCs on stiffer mats maintained spread morphology (A: 13 cm- day 1, B: day 5, C: day 10), but on flexible mats assumed rounded morphology (D: 30 cm- day 1, E: day 5, F: day 10). G: after 15-16 days firm aggregates developed, with some cells migrating towards aggregate

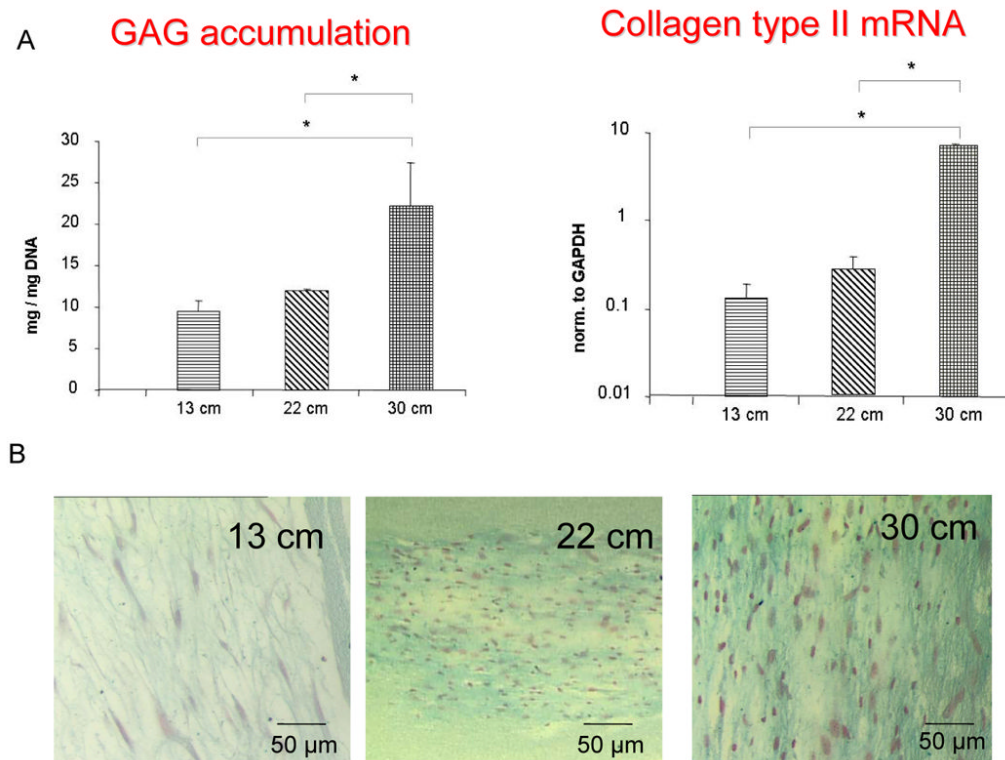
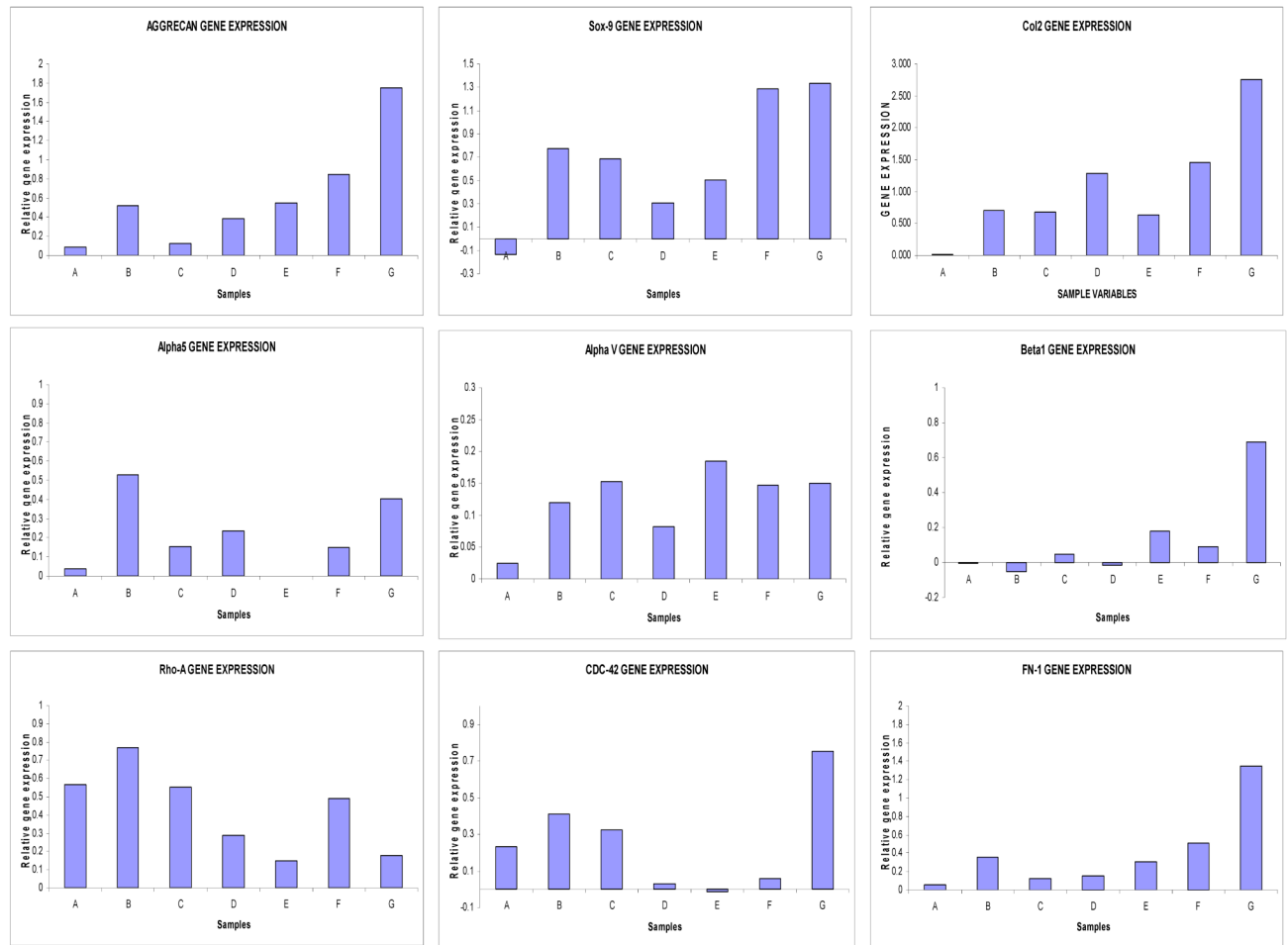


Figure 4.

Actin (red), vinculin (green) expression of hMSCs cultured over nanofibrous mats: Upper panels: A: strong actin cytoskeletal expression on rigid matrix, B: punctuated actin cytoskeleton over loose nanofibrillar matrix, Lower panels: C: vinculin focal adhesion points uniformly distributed in MSCs grown over rigid mat, D: vinculin is clustered around periphery of the cells grown over flexible mat, indicating chondrogenic differentiation



A=13-DAY5 : B= 13-DAY21 : C= 22-DAY5 : D= 22-DAY21 : E= 30-DAY5 : F= 30-DAY14 : G= 30-DAY21

Figure 5.

A: accumulation of glucosaminoglycan normalized to DNA content, and Collagen type II mRNA expression by different nanofibrous matrixes, B: Alcian blue staining showing modulation of cell morphology and staining intensity

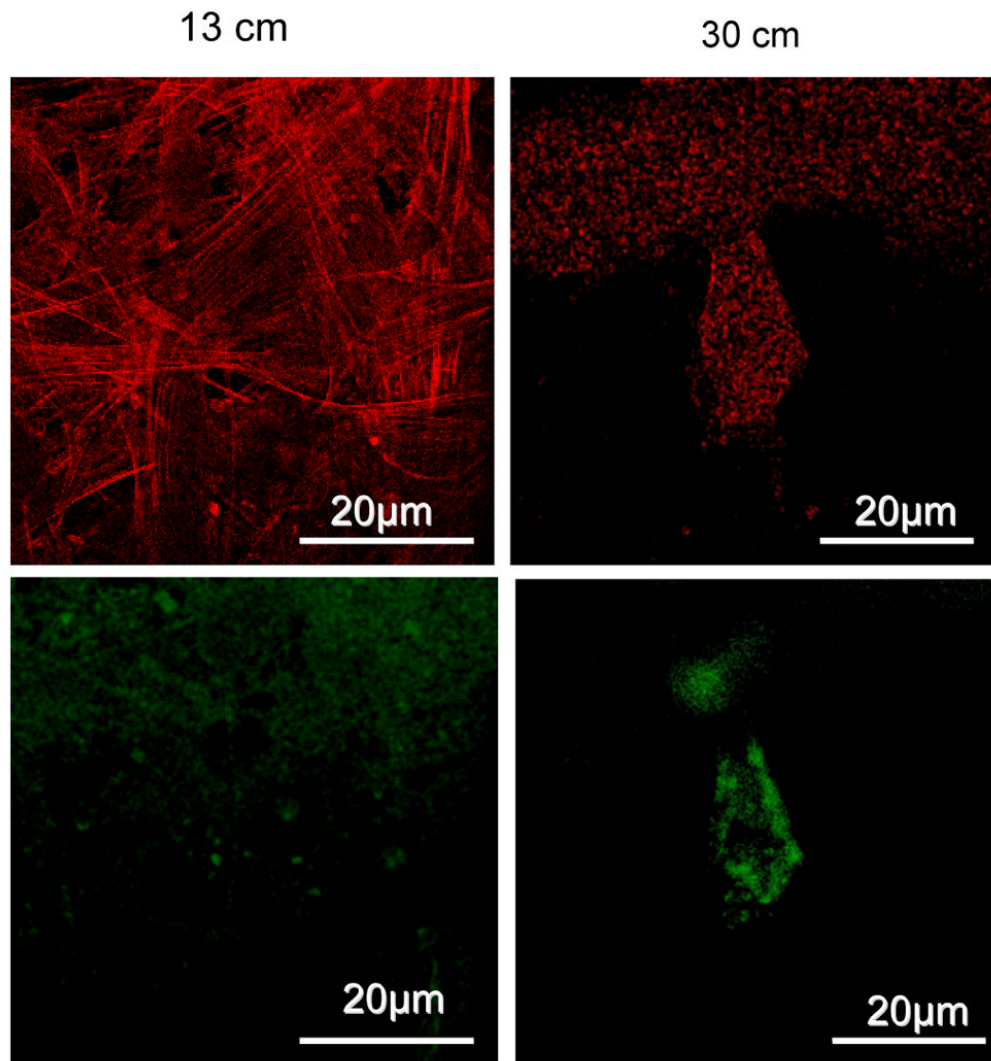


Figure 6. Chondrogenic gene expression profiling at different time point of culture, A=13 cm mat-Day 5, B= 13 cm mat-Day 21, C= 22 cm mat-Day 5, D= 22 cm mat-Day 21, E= 30 cm mat-Day 5, F= 30 cm mat-Day 14, G= 30 cm mat-Day 21

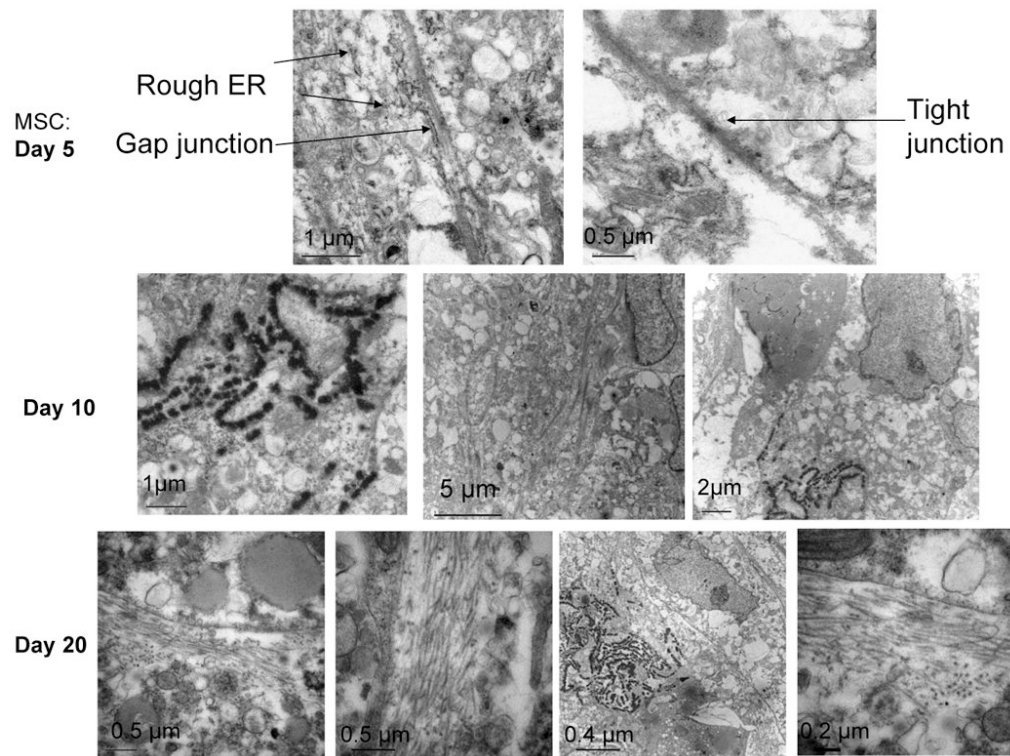


Figure 7. TEM pictures of hMSCs grown over flexible nanofibrous mats undergoing close cell-cell contact (A: day 5), enhanced pericellular matrix production (B: day 10), accumulation of collagen fibers and electron dense ECM products (C: day 20)

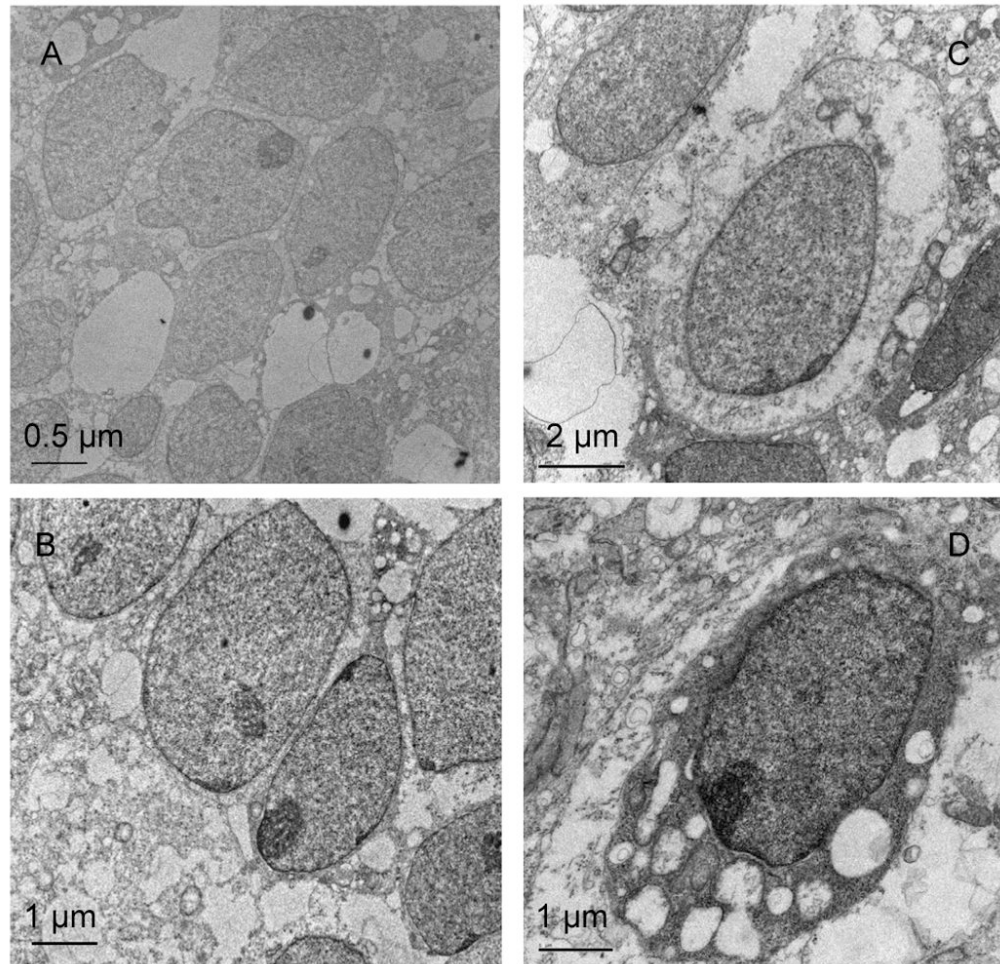


Figure 8.

TEM pictures of human embryonic stem cells on flexible mat: After day 2: close cell-cell contacts throughout aggregates (A, B), After day 10: separation of cells by pericellular ECM components (C), assuming oval 'chondron'-like structures, abundant fragmented collagen fibers (D)